The wasting-associated oncometabolite succinate disrupts myogenesis and impairs skeletal muscle regeneration

Paige C Arneson[1], Kelly A Hogan[1], Alexandra M Shin[1], Adrienne Samani[1], Aminah Jatoi[2], Jason D Doles[1]*

[1]Department of Biochemistry and Molecular Biology, Mayo Clinic, Rochester, Minnesota, 55905 USA. [2]Department of Oncology, Mayo Clinic, Rochester, Minnesota.

*Corresponding Author:
Jason D Doles
Department of Biochemistry and Molecular Biology
Mayo Clinic
200 First St SW
Guggenheim 16-11A1
Rochester, MN 55905
Tel: (507) 284-9372
Fax: (507) 284-3383
E-mail: Doles.Jason@mayo.edu

ABSTRACT

Background: Loss of muscle mass and function are major clinical phenomena affecting most advanced cancer patients. Recent work shows that defects in muscle regeneration contribute to cancer-associated wasting. Among the factors implicated in wasting-associated suppression of muscle regeneration are cytokines that interfere with myogenic signal transduction pathways. Less understood is how other cancer/wasting-associated cues, such as oncometabolites, contribute to muscle dysfunction. This study investigates how the oncometabolite succinate affects myogenesis and muscle regeneration.

Methods: We leveraged an established ectopic metabolite treatment strategy to evaluate the ability of intracellular succinate elevation to 1) affect myoblast homeostasis (growth/proliferation, apoptosis), 2) stimulate wasting-associated catabolism, and 3) modulate *in vitro* myogenesis. *In vivo* succinate supplementation experiments were utilized to corroborate and extend *in vitro* observations. Metabolic studies were then performed to investigate the impact of succinate elevation on mitochondria function.

Results: We found that *in vitro* succinate elevation in myoblasts interferes with protein homeostasis and myogenic differentiation. Mice orally administered succinate displayed smaller muscle myofiber diameters and exhibited impaired skeletal muscle regeneration when challenged with barium chloride-induced muscle injury. Finally, we found that succinate elevation was associated with functional mitochondria deficits.

Conclusions: Overall, this study broadens the repertoire of wasting-associated factors that can directly modulate muscle progenitor cell function and strengthens the hypothesis that metabolic derangements are major contributors to cancer-associated muscle wasting.

Keywords: Muscle wasting, skeletal muscle, succinate, myogenesis

INTRODUCTION

Lean mass (muscle) loss and functional skeletal muscle decline affect the majority of advanced cancer patients and are associated with poor prognosis and quality of life. Reversing muscle loss in tumor-bearing animal models leads to improved chemotherapeutic efficacy, reduced cancer-associated morbidity, and prolonged survival[1,2], demonstrating that maintaining muscle mass in cancer patients should be a top clinical priority. Despite a growing number of active clinical trials for cancer-associated weight loss, effective therapies remain elusive. Major problems hampering significant progress include the variability of weight loss presentation across tumor types and stages, limited early detection of lean mass/adipose tissue loss, and a poor understanding of the molecular underpinnings of this complex syndrome. More work is needed to identify and target alterations in skeletal muscle that contribute to overall tissue decline in cancer patients.

Multiple factors produced by both tumor and host contribute to the wasting state. Many identified 'wasting factors' are cytokines/chemokines such as TNF-alpha, Interleukins (including IL-1 and IL-6), CXC-proteins, and TGF-β[3-6], and are known to accelerate muscle atrophy, promote protein breakdown, and inhibit muscle regeneration. Additionally, many of these factors are linked to mitochondria dysfunction and altered cellular metabolism[7]. Indeed, metabolic regulation of skeletal muscle function has come into focus as a major driver of multiple aspects of muscle biology including catabolism, hypertrophy, and regenerative capacity. Examples of metabolic processes linked to cancer-associated muscle wasting are: mitochondria dynamics[8], mitochondria biogenesis[9,10], mitochondria catabolism (ie. mitophagy)[11], and compromised energy utilization pathways[12]. A more sophisticated understanding of how metabolic factors contribute to cancer-associated muscle dysfunction is needed to facilitate the development of novel therapies to preserve muscle mass and function in cancer patients.

57 Succinate is an oncometabolite best known for its role as a TCA cycle
58 intermediate and central player in mitochondria metabolism and ATP generation.
59 Recently, new roles for succinate have emerged and include immune cell
60 modulation[13], HIF-1a stabilization in cancer[14], epigenome remodeling via
61 inhibition of alpha-ketoglutarate dependent dioxygenases[15], and post-
62 translational protein modification (succinylation)[16]. This expanding repertoire of
63 cellular activities suggests a broader role for succinate in regulating cellular
64 processes such as differentiation, fate decisions, and survival. Interestingly, a
65 recent study reported serum succinate accumulation as a biomarker capable of
66 distinguishing non-wasting, tumor-bearing, and tumor-bearing with weight loss
67 patients[17]. In the present study, we sought to determine if succinate elevation
68 directly impacts muscle cell function, with a particular emphasis on myogenic
69 differentiation given prior studies linking succinate levels to cell fate
70 decisions[18,19].

71 Alterations in the balance between muscle breakdown and
72 repair/regeneration underlie cancer-associated muscle wasting. While catabolic
73 pathways have historically received the most attention in the muscle wasting
74 field, processes leading to the suppression of muscle regeneration are
75 understudied despite their clear contribution to the etiology of muscle wasting[20].
76 Central to the process of muscle regeneration is the skeletal muscle stem cell, or
77 satellite cell. In healthy muscle, satellite cells contribute to tissue maintenance
78 and actively participate in muscle homeostasis[21,22]. When challenged by injury
79 stimuli, satellite cells activate, proliferate, and differentiate into mature muscle
80 cells in order to facilitate muscle repair and regeneration. Indeed, genetic
81 ablation experiments show that Pax7+ stem/satellite cells are required for muscle
82 regeneration following major trauma[23-25]. Defects in satellite cell function and/or
83 regeneration are associated with a growing list of muscle atrophy states including
84 disuse[26,27], denervation[28,29], chronic obstructive pulmonary disease (COPD) [30],
85 burn injury[31,32], diabetes[33,34], chronic kidney disease[35], and hepatic disorders[36].
86 In cancer, multiple studies show that muscle regeneration is linked to functional
87 skeletal muscle deficits and propose that mononuclear muscle progenitor cells

88 drive aspects of the atrophy phenotype[37,38]. Taking into account the expanding
89 role of the satellite cell in muscle wasting, the importance of metabolism in
90 cancer-associated wasting, and recent evidence implicating the oncometabolite
91 succinate in cancer cachexia[17] and stem/progenitor cell function[18,19], we sought
92 to characterize the effects of succinate elevation in muscle myoblast cells (*in*
93 *vitro*) and using animal models (*in vivo*). Studies presented herein highlight the
94 ability of an oncometabolite – succinate – to directly impact myogenesis and
95 muscle regeneration, thus underscoring the need to further explore metabolic
96 drivers of muscle wasting in order to advance anti-wasting cancer therapies.

97 **METHODS**

98 **Animals**

99 Mice were bred and housed according to NIH guidelines for the ethical treatment
100 of animals in a pathogen-free facility at the Mayo Clinic (Rochester, MN campus).
101 The Mayo Clinic Institutional Animal Care and Use Committee (IACUC) approved
102 all animal protocols and all experiments were performed in accordance with
103 relevant guidelines and regulations. Wild type mice were on the FVB background
104 (Charles River Labs) unless noted otherwise in the text or figure legends. For
105 homeostasis and regeneration assays, all mice were 3-5 months old, FVB males.
106 In these experiments, mice were administered succinate (Sigma-Aldrich) (2%)
107 and 1% sucrose (vehicle) or 1% sucrose (vehicle only) in their drinking water for
108 6-8 weeks prior to and throughout the injury time course. Muscle injury was
109 performed by injecting the left *tibialis anterior* muscle with 70uL $BaCl_2$ (1.2% in
110 saline) or saline (control) and harvesting muscles 1 or 4 weeks post injury.

111 **MRI imaging**

112 An EchoMRI (magnetic resonance imaging) Body Composition Analyzer (Echo
113 Medical Systems, Houston, USA) was used for longitudinal body composition
114 analyses. Mice were scanned twice weekly for the 6-week duration of the
115 succinate water experiments. All body composition analyses were performed in
116 the accompanying EchoMRI software. Mice were weighed on a standard, digital
117 lab scale prior to scanning.

118 **Cell culture**

119 C2C12 cells (ATCC CRL-1772) were grown on tissue culture treated dishes in
120 growth media consisting of high glucose DMEM media supplemented with 10%
121 fetal bovine serum and 1% penicillin/streptomycin. Differentiation-inducing media
122 contains 2% horse serum in place of 10% fetal bovine serum. Differentiating
123 cultures were maintained by alternating fresh media additions and complete
124 media changes on a daily basis for 5 days. DM-succinate (Sigma-Aldrich) was
125 added directly to the culture media upon switching to differentiation media at

126 doses of 4 or 8 mM. Live cell analyses: Cell proliferation and cell death were
127 measured by live cell analysis (Incucyte S3 Live-Cell Imaging System, Essen
128 Bioscience). Percent apoptotic cells over a 48h time course was determined by
129 labeling control or treated cultured C2C12 cells with a phosphatidylserine
130 cyanine fluorescent dye (Annexin V Red Reagent, Essen Bioscience) according
131 to the manufacturer.

132 **Immunostaining**

133 Tissue for immunostaining was placed in a sucrose sink (30%) overnight prior to
134 freezing and sectioning. Sections (8-10 um) were post-fixed in 4%
135 paraformaldehyde (PFA) for 5 minutes at room temperature prior to
136 immunostaining. Once fixed, tissue sections were permeabilized with 0.5%
137 Triton-X100 in PBS followed by blocking with 3% BSA, 0.2% Triton-X and 0.2%
138 Tween-20 in PBS. Primary antibody incubations occurred at RT for 90 minutes
139 followed by incubation with secondary antibody at RT for 30 minutes in buffer
140 described above. The following antibodies were used in this study: MF-20
141 (Developmental Hybridoma Bank), Laminin (Sigma 4HB-2), and BF-F3
142 (Developmental Hybridoma Bank), and SC-71 (Developmental Hybridoma Bank),
143 Pax7 (Developmental Hybridoma Bank), Ki67 (Santa Cruz) and Myogenin (Santa
144 Cruz). Secondary antibodies were all Alexa fluorescent conjugates (488, 555, or
145 647) from Invitrogen or Jackson ImmunoResearch.

146 **Flow cytometry**

147 OPP assay: C2C12 myoblasts were grown to 60% confluency prior to treatment
148 with either control media or 8 mM succinate media for 48 hours. N= 3 plates
149 control, n=3 8mM succinate. Cells were incubated with O-Propargyl-Puromycin
150 (OPP) for 1.5 hours and then trypsinized and stained following the
151 manufacturer's instructions (protein synthesis assay kit (Cayman Chemical
152 #601100)). Viobility 405/452 fixable dye (Miltenyi Biotec 130-110-205) was used
153 as live/dead discriminator. After staining, cells were immediately analyzed by flow
154 cytometry on a MACSquant 10 analyzer (Miltenyi Biotec). Data were analyzed
155 using MACSquantify software (Miltenyi Biotec).

156 **Quantitative RT-qPCR**

157 C2C12 cells were differentiated as described above and cell pellets were
158 collected at each day post differentiation as well as prior to differentiation (day 0,
159 growth media). RNA was isolated using column purification (Qiagen) and cDNA
160 was prepared using high capacity cDNA reverse transcription kit (Applied
161 Biosystems). qPCR was preformed using BioRad CFX384 Real Time System.
162 Primer sequences are available upon request.

163 **Metabolic Assays**

164 A Seahorse XFe24 Analyzer (Agilent) was used to perform mitochondria stress
165 tests and energy phenotyping tests on C2C12 cells. Cells were treated with 4 or
166 8mM DM-succinate or control growth media for 16-18 hours prior to the assay.
167 DM-succinate treatment was maintained throughout the assay. Oligomycin (1
168 μM), FCCP (0.4 μM) and rotenone/antimycin A (1 μM, 1 μM) were used to inhibit
169 mitochondria complexes involved in electron transport/ATP production. Prior to
170 start of the assay, total cells/well counts were obtained on a Celigo imaging
171 cytometer (Nexcelom Bioscience) using Hoechst 33342 stain (Thermofisher). All
172 data were normalized to Celigo counts of cells/well. Wave software (Agilent,
173 version 3.0.11) was used in the analysis of energy phenotyping data.

174 **Quantitative metabolite analyses**

175 Sample preparation: Cells were treated for 48 hours with 4 or 8 mM DM-
176 succinate, washed 3 times with PBS, and stored at -80C until metabolite
177 extraction. Muscle tissue was cut into ~50 mg pieces, flash frozen in liquid
178 nitrogen, and stored at -80 C until metabolite extraction. Conditioned media was
179 flash frozen in liquid nitrogen. All samples were submitted to the Mayo Clinic
180 Metabolomics Resource Core for targeted metabolomics.

181 TCA: Concentration of TCA analytes were measured by gas chromatograph
182 mass spectrometry (GC/MS) as previously described with a few modifications[39].
183 Briefly, cell culture supernatants were spiked with internal solutions containing U-
184 ^{13}C labeled analytes. Proteins were removed by adding 250 ul of chilled

185 methanol and acetonitrile solution to the sample mixture. After drying the
186 supernatant in the speed vac, the sample was derivatized with ethoxime and
187 then with MtBSTFA + 1% tBDMCS (N-Methyl-N-(t-Butyldimethylsilyl)-
188 Trifluoroacetamide + 1% t-Butyldimethylchlorosilane) before it was analyzed on
189 an Agilent 5975C GC/MS (gas chromatography/mass spectrometry) under
190 electron impact and single ion monitoring conditions. Concentrations of lactic
191 acid (m/z 261.2), fummaric acid (m/z 287.1), succinic acid (m/z 289.1),
192 oxaloacetic acid (m/z 346.2), ketoglutaric acid (m/z 360.2), malic acid (m/z
193 419.3), aspartic acid (m/z 418.2), 2-hydroxyglutaratic acid (m/z 433.2), cis-
194 aconitic acid (m/z459.3), citric acid (m/z 591.4), and isocitric acid (m/z 591.4),
195 glutamic acid (m/z 432.4) were measured against a 7-point calibration curves
196 that underwent the same derivatization. n=1 for each supernatant sample, which
197 was run in 2 technical replicates after derivatization.

198 **Untargeted metabolomics analyses**

199 Three biological replicates of control and DM-succinate (8 mM) treated C2C12
200 cells were prepared for untargeted metabolomics analyses as follows: cells were
201 grown to 60% confluency and then treated with 8 mM succinate for 48 hours, at
202 which time plates were washed with PBS and cells were scraped and pelleted,
203 followed by storage at -80° C. Samples were submitted to the Metabolomics
204 Core at Mayo Clinic (Rochester, MN, USA) for metabolomics profiling by liquid
205 chromatography-mass spectrometry (LC/MS) using 6550 iFunnel Quadrupole
206 Time of Flight (Q-TOF) mass spectrometer (Agilent). Metabolites were then
207 identified using METLIN database with Mass Profiler Professional software
208 (Agilent). Annotated metabolites with a p value less than 0.05 and a fold change
209 greater than 2 were further analyzed using MetaboAnalyst network explorer[40]
210 (metabolite-metabolite interactions) and enrichment analysis (pathway
211 associated metabolite sets) tools. KEGG and HMDB identifiers were used in
212 MetaboAnalyst.

213 **RNA sequencing analysis**

214 Sample/library preparation: Three biological replicates of control and DM-
215 succinate (8mM) treated C2C12 cells were prepared for untargeted
216 metabolomics analyses as follows: cells were grown to 60% confluency and then
217 treated with 8mM succinate for 48 hours, at which time plates were washed with
218 PBS and cells were scraped and pelleted, followed by storage at -80° C. Frozen
219 cell pellets were submitted to the Mayo Clinic Medical Genome Facility where
220 RNA quality was determined using the Fragment Analyzer from AATI. RNA
221 samples that have RQN values ≥6 were approved for library prep and
222 sequencing. RNA libraries were prepared using 200 ng of good quality total RNA
223 according to the manufacturer's instructions for the TruSeq RNA Sample Prep Kit
224 v2 (Illumina, San Diego, CA), employing poly-A mRNA enrichment using oligo dT
225 magnetic beads. The final adapter-modified cDNA fragments were enriched by
226 12 cycles of PCR using Illumina TruSeq PCR primers. The concentration and
227 size distribution of the completed libraries were determined using a Fragment
228 Analyzer (AATI, Ankeny, IA) and Qubit fluorometry (Invitrogen, Carlsbad, CA).
229 Libraries were sequenced following Illumina's standard protocol using the
230 Illumina cBot and HiSeq 3000/4000 PE Cluster Kit, yielding approximately 48-70
231 million fragment reads per sample. The flow cells were sequenced as 100 X 2
232 paired end reads on an Illumina HiSeq 4000 using HiSeq 3000/4000 sequencing
233 kit and HCS v3.3.52 collection software. Base-calling was performed using
234 Illumina's RTA version 2.7.3. Bioinformatics/Data Processing: All bioinformatics
235 analyses were done through the Mayo Clinic Bioinformatics Core. The raw RNA
236 sequencing paired-end reads for the samples were processed through the Mayo
237 RNA-Seq bioinformatics pipeline, MAP-RSeq version 3.0.0[41]. Briefly, MAP-RSeq
238 employs the splice-aware aligner, STAR[42], to align reads to the reference mouse
239 genome build mm10. Gene and exon expression quantification were performed
240 using the Subread[43] package to obtain both raw and normalized (RPKM – Reads
241 Per Kilobase per Million mapped reads) reads.

242 **Statistics**

243 Data are represented as the mean ± SD using GraphPad Prism unless noted
244 otherwise in the figure legends. Quantification of nuclei per MyHC+ structure was
245 analyzed using nonparametric, Mann-Whitney t-tests. Quantification of muscle
246 cross sections using minimum feret diameter measurements was analyzed by
247 non-linear regression (gaussian, least squares method) and compared between
248 conditions using an extra sum-of-squares F test. All other comparisons between
249 groups were performed using unpaired two-tailed student's t tests or multiple t
250 tests with Holm-Sidak multiple testing correction, as noted in figure legends. For
251 all analyses, a $p<0.05$ was considered significant (denoted with *); a $p<0.01$ was
252 denoted with ** unless noted otherwise in the figure legend.

253 **Data availability**

254 Datasets generated during the current study are available from the
255 corresponding author upon request.

256 **RESULTS**

257 Modeling succinate accumulation and evaluating consequences on growth and
258 atrophy

259 To evaluate the effects of succinate on *in vitro* myoblast function, we first
260 sought to adapt an established paradigm of intracellular succinate accumulation
261 for use in myoblast cells. Succinate has very low cell permeability *in vitro*, so we
262 began our studies using dimethyl-succinate (DM-succinate or DMS), a cell
263 permeable succinate analog used in prior studies to elevate intracellular
264 metabolite levels[18,19]. We treated proliferating C2C12 myoblasts for 48 hours with
265 two concentrations of DM-succinate, 4 mM and 8 mM, and then performed
266 targeted metabolomics to quantify levels of TCA cycle-associated metabolites.
267 We found that 8 mM DM-succinate treatment resulted in a significant increase in
268 intracellular succinate (~2.5-fold) compared to control treatment, similar in
269 magnitude to previously reported values[18] and consistent with the degree of
270 succinate accumulation in wasting cancer patients[17]. We did not detect
271 statistically significant changes in most other TCA metabolites analyzed, with the
272 exception of small (<2 fold) but significant increases in malate and glutamate
273 (**Fig. 1A**). We chose to evaluate this dosing paradigm further to investigate the
274 effects of intracellular succinate elevation on myogenesis. Cell proliferation and
275 apoptosis are important regulators of myogenesis. To test if succinate would
276 influence either of these processes, we evaluated cells treated with three doses
277 of DM-succinate over 48 hours. We did not see significant differences in
278 proliferation over this time period, and only saw increased apoptosis rates with
279 16 mM DM-succinate treatment (**Fig. 1B, C**).

280 A major feature of cancer-associated muscle wasting is myofiber atrophy due
281 to either enhanced protein catabolism or impaired protein anabolism. In
282 myoblasts exposed to DM-succinate, we did not observe an increase in mRNA
283 transcripts encoding for E3 ubiqutin ligases (MuRF1, Atrogin-1) typically
284 associated with enhanced muscle catabolism (**Fig. 1D**). We did, however,
285 observe a reduction in protein anabolism as determined by an O-propargyl-

286 puromycin (OPP) incorporation assay, performed in proliferating C2C12
287 myoblasts treated with 8 mM DM-succinate for 48 hours (**Fig. 1E**). Interestingly,
288 differentiated C2C12 myotubes treated with 8 mM DM-succinate for 24 hours
289 post myogenic differentiation did not exhibit statistically significant alterations in
290 mean myotube diameter (**Fig. 1F**), suggesting that the DM-succinate-associated
291 protein anabolism deficits are not sufficient to drive muscle atrophy.

292 Elevated succinate levels impair *in vitro* myogenesis

293 To gain a more comprehensive understanding of the molecular changes
294 associated with succinate elevation, we performed RNA sequencing (RNA-seq)
295 on proliferating C2C12 myoblasts treated with 8 mM DM-succinate for 48 hours.
296 Analysis of the transcripts involved in myogenesis and lineage specification
297 revealed widespread transcript down-regulation after exposure to DM-succinate
298 (**Fig. 2A**). These results led us to more closely investigate myogenic progression
299 by differentiating C2C12 myoblast cultures in low serum conditions for 5 days in
300 the presence or absence of 8 mM DM-succinate. In this assay, we assessed the
301 degree of terminal differentiation by quantitative RT-PCR analysis of myogenic
302 transcript expression (Pax7, MyoD1, Myog, and MyH1) and the number of nuclei
303 fused into differentiated, Myosin Heavy Chain-positive myocytes/myotubes.
304 Analysis of key myogenic transcript expression patterns supported the RNA-seq
305 data, showing downregulation of MyoD1, Myog and MyH1, particularly earlier in
306 the differentiation time course (**Fig. 2B**). Although not statistically significant,
307 Pax7 expression was trending upwards in DM-succinate-treated cells (**Fig. 2B**).
308 Differentiating C2C12 cells in the presence of 8 mM DM-succinate resulted in an
309 impaired ability to form mature, multinucleated Myosin Heavy Chain-positive
310 structures (control, 4 mM DM-succinate, 8 mM DM-succinate mean
311 nuclei/myotube values = 5.43, 4.62, 2.98, respectively; **Fig. 2C, D**). Together,
312 these data show that elevated succinate in muscle cells influences protein
313 anabolism and suppresses myogenic differentiation and that these changes are
314 distinct from direct myotube atrophy via enhanced protein catabolism.

315 *In vivo* succinate supplementation impairs skeletal muscle homeostasis

316 Defects in progenitor cell activation, expansion, differentiation, or fusion
317 compromise the regenerative capacity of skeletal muscle. Given our observations
318 that DM-succinate impairs myogenic differentiation *in vitro*, we next asked if
319 succinate supplementation negatively impacts *in vivo* skeletal muscle
320 homeostasis. Wildtype mice were either supplemented with vehicle (1% sucrose)
321 control drinking water or water with 2% succinate (+1% sucrose vehicle). We
322 found that there was no significant difference in total body weight across the
323 supplementation, or at the endpoint (**Fig. 3A, B**). In addition to total body weight,
324 we longitudinally monitored body composition of the mice twice weekly for six
325 weeks using magnetic resonance imaging (MRI). Total lean mass, as measured
326 by MRI-based body composition analyses, did not show a difference between
327 vehicle and succinate-supplemented mice (**Fig. 3C)**. Comparisons of *tibialis*
328 *anterior* (TA) and *gastrocnemius* (GR) muscle wet weights after six weeks of
329 supplementation did not reveal significant differences between experimental
330 groups (**Fig. 3D)**. Following six weeks of succinate supplementation, we
331 harvested TA muscles and stained tissue cross sections with laminin, a protein
332 on the myofiber membrane, to evaluate myofiber size (**Fig. 3E)**. We quantified
333 myofiber minimum feret diameters using Myovision[44] and found a statistically
334 significant decrease in the non-linear regressions fit to the histograms of
335 minimum feret diameter distribution between control and succinate supplemented
336 cohorts (**Fig. 3F)**.

337 Succinate supplementation impairs skeletal muscle regeneration

338 Muscle progenitor cells are required for efficient muscle regeneration
339 following serious injury[23-25]. In order to challenge resident satellite cells
340 chronically exposed to elevated succinate, after six weeks of supplementation,
341 we injured TA muscles with intramuscular barium chloride injection (1.2%). At 7
342 days and 28 days post injury (dpi) we harvested TA muscle for histological
343 analysis. At 7 dpi, we observed statistically significant ($p=0.0016$) differences in
344 myofiber regeneration as evidenced by ~16% reduction in the mean of non-linear
345 regression curves fit to the minimum feret diameter distribution (**Fig. 4A, B**).
346 Muscle regeneration post barium chloride injury is typically completed four weeks

347 post injury in healthy, adult mice. When we analyzed minimum feret diameters at
348 28 dpi, the difference in the mean of non-linear regression curves fit to the
349 minimum feret diameter distribution became more pronounced (~52% reduction,
350 $p<0.0001$) (**Fig. 4C, D**). Injured TA muscle in succinate supplemented mice
351 exhibited large areas of poorly regenerated tissue (**Fig. 4C**). To further
352 investigate the impacts of chronic succinate supplementation on the satellite cell
353 population we looked at markers of myogenic differentiation and proliferation. We
354 saw no significant difference in the number of total (PAX7+) or proliferating
355 (PAX7+KI67+) muscle progenitor cells in succinate-supplemented animals at 7-
356 or 28 dpi, in concordance with *in vitro* proliferation data (**Fig. 4E, F; top**). At 7-
357 days post injury there was no difference in the number of MYOG+ differentiating
358 muscle progenitor cells between succinate- and vehicle-supplemented mice.
359 However, we did see a significant accumulation of differentiating muscle
360 progenitor cells (MYOG+) in succinate-supplemented animals at 28 dpi,
361 indicative of stalled or incomplete myogenesis. In comparison, vehicle-
362 supplemented mice had low numbers of MYOG+ cells at 28 dpi likely due to
363 effective completion of myogenesis (**Fig. 4E; bottom**). Taken together, these
364 data show that succinate supplementation alters progenitor cell dynamics
365 resulting in impaired skeletal muscle homeostasis and diminished skeletal
366 muscle regeneration.

367 Succinate elevation disrupts multiple metabolic networks in muscle cells

368 Succinate is gaining traction as a metabolite capable of acting as more than a
369 substrate for succinate dehydrogenase and the respiratory chain[45]. Notably,
370 succinate is located at the intersection of many diverse metabolic pathways and
371 can influence a wide range of metabolic processes[46,47]. We performed non-
372 targeted metabolomics profiling on control and 8 mM treated (48h) C2C12
373 myoblasts and found a striking number of differentially abundant metabolites
374 (DAMs) between in the two conditions (214 features with $p<0.05$, FC>2). Network
375 analyses of metabolic pathways associated with these DAMs implicated
376 pathways involved in amino acid and nucleotide metabolism, as well as
377 metabolic processes associated with mitochondrial metabolism and the TCA

378 cycle (**Fig. 5A,B**). Considering the central role of the mitochondria in coordinating
379 cellular metabolism and the known involvement of succinate in several
380 mitochondria-coupled processes, we posited that succinate elevation could result
381 in mitochondria dysfunction. Prior evidence suggests that myogenic
382 differentiation involves metabolic rewiring characterized by increased
383 mitochondria mass and a shift towards oxidative phosphorylation[48,49]. To assess
384 mitochondria function, we measured cellular oxygen consumption rates (OCR) in
385 proliferating myoblasts treated with 4 mM and 8 mM DM-succinate exposed to
386 mitochondrial stressors. When treated with compounds targeting ATP synthase
387 (oligomycin), the hydrogen ion gradient (FCCP), and complex I/III
388 (Rotenone/Antimycin A), we noted altered OCR dynamics in myoblasts treated
389 with the highest dose (8 mM) of DM-succinate (**Fig. 5C**). Maximal respiration, as
390 determined by OCR measurements following the addition of the ionophore
391 FCCP, was significantly reduced (~35%) in the presence of 8 mM DM-succinate
392 (**Fig. 5D**), thus significantly decreasing mitochondria reserve capacity[50] (~50%
393 reduction; **Fig. 5E**). Basal respiration rates, and non-mitochondrial respiration
394 were unaffected by succinate elevation (**Fig. 5F, G**). The ability of cells to
395 respond to general mitochondrial stress was further assessed using an energy
396 phenotyping test, which exposes cells to FCCP and oligomycin simultaneously
397 and measures both ECAR (extracellular acidification rate) and OCR. When
398 stressed, control cells exhibited expected increases in ECAR and OCR, whereas
399 DM-succinate treated cells responded poorly (**Fig. 5H**). Taken together, these
400 data show that while elevated succinate does not grossly affect mitochondria
401 morphology or basal (resting) respiration parameters, it does impact the ability of
402 cells to maximally engage mitochondrial respiration under stressful conditions.

403 **DISCUSSION**

404 Mitochondria and tricarboxylic acid (TCA) cycle defects are commonly
405 observed in wasting skeletal muscle[51-53]. Direct alterations to TCA metabolite
406 stoichiometry could therefore, in principal, contribute to functional deficits
407 associated with muscle wasting. Indeed, multiple studies show that perturbations
408 in the succinate/alpha-ketoglutarate ratio underlie a spectrum of cellular defects
409 ranging from epigenome alterations to mitochondria deficits[15,19,54]. In this study,
410 we found that succinate elevation in muscle progenitor cells impaired myogenic
411 differentiation *in vitro* and disrupted *in vivo* muscle regeneration in response to
412 injury. While we did not explore the wasting-inducing potential of other
413 metabolites, we anticipate that future evaluation of metabolites as wasting-
414 associated factors will reveal many new drivers of muscle wasting and will
415 prompt a re-evaluation of therapeutic strategies designed to limit cancer-
416 associated weight loss.

417 Several groups show that elevated succinate can influence multiple metabolic
418 processes including NADH/NAD+ redox state, phosphate metabolism, carbon
419 source utilization, amino acid incorporation, and fatty acid synthesis[46,47,55,56]. Of
420 note, succinate CoA ligase (SUCL) – which catalyzes succinyl-CoA and
421 ADP/GDP to CoASH, succinate, and ATP/GTP – is subject to inhibition by the
422 accumulation succinate[45]. This product inhibition of SUCL could lead to a buildup
423 of upstream CoA species such as propionyl-CoA and methylmalonyl-CoA, which
424 in turn would likely inhibit the catabolism of many macromolecules that are
425 normally metabolized to succinyl-CoA, including branched-chain amino acids,
426 cholesterol, propionate, and odd-chain fatty acids[57,58]. Future studies focusing on
427 how succinate engages other metabolic networks will help to clarify how elevated
428 succinate levels result in impaired muscle repair/regeneration and contribute to
429 cancer-associated muscle wasting.

430 Recent work shows that mitochondria and energy homeostasis play important
431 roles in the regulation of myogenesis. A study that measured the relative
432 contribution of oxidative phosphorylation (OXPHOS) to total cellular ATP in

433 muscle cells demonstrates a shift from ~30% OXPHOS dependent ATP
434 production in proliferating myoblasts to ~60% in terminally differentiated
435 myotubes[59]. Accordingly, mRNA expression profiles and activities of
436 mitochondrial enzymes including citrate synthase, isocitrate dehydrogenase, 3-
437 hydroxyacyl-CoA dehydrogenase, cytochrome oxidase, NADH dehydrogenase,
438 and succinate dehydrogenase are markedly increased during myogenic
439 differentiation[60]. Several lines of evidence show that functional impairment of
440 mitochondria negatively regulates myogenic differentiation. First, mitochondrial
441 protein synthesis inhibition by chloramphenicol impaired chick embryo myoblast
442 fusion, even when proliferation/apoptosis rates were maintained by tryptose
443 phosphate broth or nucleoside supplementation[61]. Second, over-expression of
444 key factors involved in mitochondria biogenesis (PGC-1 genes) in skeletal
445 muscle enhanced mtDNA content, mitochondrial enzyme activities, and exercise
446 performance[62], whereas mice lacking PGC-1 show reduced mitochondria
447 numbers, decreased expression of mitochondrial genes, and diminished muscle
448 function[63,64]. We found that while DM-succinate impaired the maximal respiratory
449 capacity of myoblasts, DM-succinate failed to affect basal mitochondria
450 bioenergetics parameters or gross mitochondria morphology. Accordingly,
451 proliferation and apoptosis rates were unchanged in DM-succinate treated cells.
452 These data support the hypothesis that elevated succinate levels specifically
453 impair myogenic differentiation, an energetically demanding process that
454 challenges myoblast mitochondria. Furthermore, these studies provide evidence
455 that suppression of myogenesis is a contributing factor to cancer-associated lean
456 mass loss.

457 Our data show that *in vivo* succinate supplementation impairs muscle
458 morphometric parameters and regeneration properties, thus adding to the
459 growing list of studies that report metabolite-driven skeletal muscle mass and/or
460 functional alterations[65,66]. Cancer-associated lean mass loss is widely considered
461 a metabolic disorder with complex and overlapping mechanisms of action that
462 ultimately lead to a decline in skeletal muscle mass and function. While cytokines
463 and chemokines have garnered the most attention as drivers of muscle wasting

464 phenotypes, our data underscore the importance of metabolites as regulators of
465 muscle function. Unfortunately, efforts to target, block or neutralize specific
466 wasting factors have seen little success[67-69]. Given the multifaceted nature of
467 cancer-associated lean mass loss, perhaps a more practical approach would be
468 to focus on the progenitor cell and/or mature muscle response to the wasting
469 environment. Such an approach would, in theory, circumvent the redundancy of
470 upstream wasting factors and open up new therapeutic avenues to limit muscle
471 wasting in cancer.

ACKNOWLEDGEMENTS

The authors wish to thank members of the Doles lab for helpful discussions and manuscript suggestions and the Mayo Microscopy and Cell Analysis Core for experimental and technical support. J.D. was supported by the National Institutes of Health/National Institute of Arthritis, Musculoskeletal and Skin Diseases (NIH/NIAMS) R00AR66696, Mayo Clinic start-up funds, Career Development Awards from the Mayo Clinic SPORE in Pancreatic Cancer (NIH/ National Cancer Institute (NCI) CA102701) and the American Association for Cancer Research/Pancreatic Cancer Action Network, and the Glenn Foundation for Medical Research. P.C.A was supported by the Mayo Clinic Regenerative Sciences Training Program (RSTP). Metabolomics studies were made possible by the Mayo Clinic Metabolomics Resource Core through NIH/ National Institue of Diabetes and Digestive and Kidney Disease (NIDDK) U24DK10049 originating from the NIH Director's Common Fund. The authors of this manuscript certify that they comply with the ethical guidelines for authorship and publishing in the Journal of Cachexia, Sarcopenia and Muscle[70].

AUTHOR CONTRIBUTIONS

Study design: PCA, KAH, JDD. Data collection: PCA, KAH, AS, AMS. Data analysis/interpretation: PCA, KAH, JDD. Writing and editing of manuscript: PCA, KAH, AJ, JDD. All authors approved this manuscript.

492 **COMPETING INTERESTS STATEMENT**

493 The authors have no competing interests to declare.

494 **REFERENCES**

495 1 Zhou, X. *et al.* Reversal of cancer cachexia and muscle wasting by
496 ActRIIB antagonism leads to prolonged survival. *Cell* **142**, 531-543,
497 doi:10.1016/j.cell.2010.07.011 (2010).
498 2 Toledo, M. *et al.* Complete reversal of muscle wasting in experimental
499 cancer cachexia: Additive effects of activin type II receptor inhibition and
500 β-2 agonist. *Int J Cancer* **138**, 2021-2029, doi:10.1002/ijc.29930 (2016).
501 3 Pal, M., Febbraio, M. A. & Whitham, M. From cytokine to myokine: the
502 emerging role of interleukin-6 in metabolic regulation. *Immunol Cell Biol*
503 **92**, 331-339, doi:10.1038/icb.2014.16 (2014).
504 4 Onesti, J. K. & Guttridge, D. C. Inflammation based regulation of cancer
505 cachexia. *Biomed Res Int* **2014**, 168407, doi:10.1155/2014/168407
506 (2014).
507 5 Loumaye, A. *et al.* Role of Activin A and myostatin in human cancer
508 cachexia. *J Clin Endocrinol Metab* **100**, 2030-2038, doi:10.1210/jc.2014-
509 4318 (2015).
510 6 Hogan, K. A. *et al.* Tumor-derived cytokines impair myogenesis and alter
511 the skeletal muscle immune microenvironment. *Cytokine*,
512 doi:10.1016/j.cyto.2017.11.006 (2017).
513 7 VanderVeen, B. N., Fix, D. K. & Carson, J. A. Disrupted Skeletal Muscle
514 Mitochondrial Dynamics, Mitophagy, and Biogenesis during Cancer
515 Cachexia: A Role for Inflammation. *Oxid Med Cell Longev* **2017**, 3292087,
516 doi:10.1155/2017/3292087 (2017).
517 8 Carson, J. A., Hardee, J. P. & VanderVeen, B. N. The emerging role of
518 skeletal muscle oxidative metabolism as a biological target and cellular
519 regulator of cancer-induced muscle wasting. *Semin Cell Dev Biol* **54**, 53-
520 67, doi:10.1016/j.semcdb.2015.11.005 (2016).
521 9 Romanello, V. *et al.* Mitochondrial fission and remodelling contributes to
522 muscle atrophy. *EMBO J* **29**, 1774-1785, doi:10.1038/emboj.2010.60
523 (2010).
524 10 Wu, S., Zhou, F., Zhang, Z. & Xing, D. Mitochondrial oxidative stress
525 causes mitochondrial fragmentation via differential modulation of
526 mitochondrial fission-fusion proteins. *FEBS J* **278**, 941-954,
527 doi:10.1111/j.1742-4658.2011.08010.x (2011).
528 11 Bordi, M., Nazio, F. & Campello, S. The Close Interconnection between
529 Mitochondrial Dynamics and Mitophagy in Cancer. *Front Oncol* **7**, 81,
530 doi:10.3389/fonc.2017.00081 (2017).
531 12 Julienne, C. M. *et al.* Cancer cachexia is associated with a decrease in
532 skeletal muscle mitochondrial oxidative capacities without alteration of
533 ATP production efficiency. *J Cachexia Sarcopenia Muscle* **3**, 265-275,
534 doi:10.1007/s13539-012-0071-9 (2012).
535 13 Tannahill, G. M. *et al.* Succinate is an inflammatory signal that induces IL-
536 1β through HIF-1α. *Nature* **496**, 238-242, doi:10.1038/nature11986
537 (2013).

538 14 Selak, M. A. *et al.* Succinate links TCA cycle dysfunction to oncogenesis
539 by inhibiting HIF-alpha prolyl hydroxylase. *Cancer Cell* **7**, 77-85,
540 doi:10.1016/j.ccr.2004.11.022 (2005).
541 15 Xiao, M. *et al.* Inhibition of α-KG-dependent histone and DNA
542 demethylases by fumarate and succinate that are accumulated in
543 mutations of FH and SDH tumor suppressors. *Genes Dev* **26**, 1326-1338,
544 doi:10.1101/gad.191056.112 (2012).
545 16 Park, J. *et al.* SIRT5-mediated lysine desuccinylation impacts diverse
546 metabolic pathways. *Mol Cell* **50**, 919-930,
547 doi:10.1016/j.molcel.2013.06.001 (2013).
548 17 Yang, Q.-J. *et al.* Serum and urine metabolomics study reveals a distinct
549 diagnostic model for cancer cachexia. *J Cachexia Sarcopenia Muscle* **9**,
550 71-85, doi:10.1002/jcsm.12246 (2018).
551 18 TeSlaa, T. *et al.* α-Ketoglutarate Accelerates the Initial Differentiation of
552 Primed Human Pluripotent Stem Cells. *Cell Metab* **24**, 485-493,
553 doi:10.1016/j.cmet.2016.07.002 (2016).
554 19 Carey, B. W., Finley, L. W. S., Cross, J. R., Allis, C. D. & Thompson, C. B.
555 Intracellular α-ketoglutarate maintains the pluripotency of embryonic stem
556 cells. *Nature* **518**, 413-416, doi:10.1038/nature13981 (2015).
557 20 Talbert, E. E. & Guttridge, D. C. Impaired regeneration: A role for the
558 muscle microenvironment in cancer cachexia. *Semin Cell Dev Biol* **54**, 82-
559 91, doi:10.1016/j.semcdb.2015.09.009 (2016).
560 21 Pawlikowski, B., Pulliam, C., Betta, N. D., Kardon, G. & Olwin, B. B.
561 Pervasive satellite cell contribution to uninjured adult muscle fibers. *Skelet*
562 *Muscle* **5**, 42, doi:10.1186/s13395-015-0067-1 (2015).
563 22 Keefe, A. C. *et al.* Muscle stem cells contribute to myofibres in sedentary
564 adult mice. *Nat Commun* **6**, 7087, doi:10.1038/ncomms8087 (2015).
565 23 Murphy, M. M., Lawson, J. A., Mathew, S. J., Hutcheson, D. A. & Kardon,
566 G. Satellite cells, connective tissue fibroblasts and their interactions are
567 crucial for muscle regeneration. *Development* **138**, 3625-3637,
568 doi:10.1242/dev.064162 (2011).
569 24 Lepper, C., Partridge, T. A. & Fan, C.-M. An absolute requirement for
570 Pax7-positive satellite cells in acute injury-induced skeletal muscle
571 regeneration. *Development* **138**, 3639-3646, doi:10.1242/dev.067595
572 (2011).
573 25 Sambasivan, R. *et al.* Pax7-expressing satellite cells are indispensable for
574 adult skeletal muscle regeneration. *Development* **138**, 3647-3656,
575 doi:10.1242/dev.067587 (2011).
576 26 Mozdziak, P. E., Pulvermacher, P. M. & Schultz, E. Muscle regeneration
577 during hindlimb unloading results in a reduction in muscle size after
578 reloading. *J Appl Physiol (1985)* **91**, 183-190,
579 doi:10.1152/jappl.2001.91.1.183 (2001).
580 27 Mitchell, P. O. & Pavlath, G. K. Skeletal muscle atrophy leads to loss and
581 dysfunction of muscle precursor cells. *Am J Physiol Cell Physiol* **287**,
582 C1753-1762, doi:10.1152/ajpcell.00292.2004 (2004).

583 28 Viguie, C. A., Lu, D. X., Huang, S. K., Rengen, H. & Carlson, B. M.
584 Quantitative study of the effects of long-term denervation on the extensor
585 digitorum longus muscle of the rat. *Anat Rec* **248**, 346-354 (1997).
586 29 Liao, H. *et al.* [Pax7 and depletion of satellite cell pool in prolonged
587 denervated skeletal muscles of adult rats]. *Zhongguo Xiu Fu Chong Jian*
588 *Wai Ke Za Zhi* **23**, 92-96 (2009).
589 30 Langen, R. C. J. *et al.* Muscle wasting and impaired muscle regeneration
590 in a murine model of chronic pulmonary inflammation. *Am J Respir Cell*
591 *Mol Biol* **35**, 689-696, doi:10.1165/rcmb.2006-0103OC (2006).
592 31 Wu, X., Walters, T. J. & Rathbone, C. R. Skeletal muscle satellite cell
593 activation following cutaneous burn in rats. *Burns* **39**, 736-744,
594 doi:10.1016/j.burns.2012.10.016 (2013).
595 32 Corrick, K. L. *et al.* Serum from human burn victims impairs myogenesis
596 and protein synthesis in primary myoblasts. *Front Physiol* **6**, 184,
597 doi:10.3389/fphys.2015.00184 (2015).
598 33 Aragno, M. *et al.* Oxidative stress impairs skeletal muscle repair in diabetic
599 rats. *Diabetes* **53**, 1082-1088 (2004).
600 34 Krause, M. P., Moradi, J., Nissar, A. A., Riddell, M. C. & Hawke, T. J.
601 Inhibition of plasminogen activator inhibitor-1 restores skeletal muscle
602 regeneration in untreated type 1 diabetic mice. *Diabetes* **60**, 1964-1972,
603 doi:10.2337/db11-0007 (2011).
604 35 Zhang, L., Wang, X. H., Wang, H., Du, J. & Mitch, W. E. Satellite cell
605 dysfunction and impaired IGF-1 signaling cause CKD-induced muscle
606 atrophy. *J Am Soc Nephrol* **21**, 419-427, doi:10.1681/ASN.2009060571
607 (2010).
608 36 Dasarathy, S. Cause and management of muscle wasting in chronic liver
609 disease. *Curr Opin Gastroenterol* **32**, 159-165,
610 doi:10.1097/MOG.0000000000000261 (2016).
611 37 Mehl, K. A., Davis, J. M., Berger, F. G. & Carson, J. A. Myofiber
612 degeneration/regeneration is induced in the cachectic ApcMin/+ mouse. *J*
613 *Appl Physiol (1985)* **99**, 2379-2387, doi:10.1152/japplphysiol.00778.2005
614 (2005).
615 38 He, W. A. *et al.* NF-κB-mediated Pax7 dysregulation in the muscle
616 microenvironment promotes cancer cachexia. *J Clin Invest* **123**, 4821-
617 4835, doi:10.1172/JCI68523 (2013).
618 39 Dutta, T. *et al.* Impact of Long-Term Poor and Good Glycemic Control on
619 Metabolomics Alterations in Type 1 Diabetic People. *J Clin Endocrinol*
620 *Metab* **101**, 1023-1033, doi:10.1210/jc.2015-2640 (2016).
621 40 Chong, J. *et al.* MetaboAnalyst 4.0: towards more transparent and
622 integrative metabolomics analysis. *Nucleic Acids Res* **46**, W486-W494,
623 doi:10.1093/nar/gky310 (2018).
624 41 Kalari, K. R. *et al.* MAP-RSeq: Mayo Analysis Pipeline for RNA
625 sequencing. *BMC Bioinformatics* **15**, 224, doi:10.1186/1471-2105-15-224
626 (2014).
627 42 Dobin, A. *et al.* STAR: ultrafast universal RNA-seq aligner. *Bioinformatics*
628 **29**, 15-21, doi:10.1093/bioinformatics/bts635 (2013).

629 43 Liao, Y., Smyth, G. K. & Shi, W. The Subread aligner: fast, accurate and
630 scalable read mapping by seed-and-vote. *Nucleic Acids Res* **41**, e108,
631 doi:10.1093/nar/gkt214 (2013).
632 44 Wen, Y. *et al.* MyoVision: software for automated high-content analysis of
633 skeletal muscle immunohistochemistry. *J Appl Physiol (1985)* **124**, 40-51,
634 doi:10.1152/japplphysiol.00762.2017 (2018).
635 45 Tretter, L., Patocs, A. & Chinopoulos, C. Succinate, an intermediate in
636 metabolism, signal transduction, ROS, hypoxia, and tumorigenesis.
637 *Biochim Biophys Acta* **1857**, 1086-1101, doi:10.1016/j.bbabio.2016.03.012
638 (2016).
639 46 Stovell, M. G. *et al.* The effect of succinate on brain NADH/NAD(+) redox
640 state and high energy phosphate metabolism in acute traumatic brain
641 injury. *Sci Rep* **8**, 11140, doi:10.1038/s41598-018-29255-3 (2018).
642 47 Aspuria, P. P. *et al.* Succinate dehydrogenase inhibition leads to epithelial-
643 mesenchymal transition and reprogrammed carbon metabolism. *Cancer*
644 *Metab* **2**, 21, doi:10.1186/2049-3002-2-21 (2014).
645 48 Wagatsuma, A. & Sakuma, K. Mitochondria as a potential regulator of
646 myogenesis. *ScientificWorldJournal* **2013**, 593267,
647 doi:10.1155/2013/593267 (2013).
648 49 Ryall, J. G. *et al.* The NAD(+)-Dependent SIRT1 Deacetylase Translates a
649 Metabolic Switch into Regulatory Epigenetics in Skeletal Muscle Stem
650 Cells. *Cell Stem Cell* **16**, 171-183, doi:10.1016/j.stem.2014.12.004 (2015).
651 50 Divakaruni, A. S., Rogers, G. W. & Murphy, A. N. Measuring Mitochondrial
652 Function in Permeabilized Cells Using the Seahorse XF Analyzer or a
653 Clark-Type Oxygen Electrode. *Curr Protoc Toxicol* **60**, 25.22.21-16,
654 doi:10.1002/0471140856.tx2502s60 (2014).
655 51 Der-Torossian, H. *et al.* Metabolic derangements in the gastrocnemius
656 and the effect of Compound A therapy in a murine model of cancer
657 cachexia. *J Cachexia Sarcopenia Muscle* **4**, 145-155, doi:10.1007/s13539-
658 012-0101-7 (2013).
659 52 Tzika, A. A. *et al.* Skeletal muscle mitochondrial uncoupling in a murine
660 cancer cachexia model. *Int J Oncol* **43**, 886-894,
661 doi:10.3892/ijo.2013.1998 (2013).
662 53 Koopman, R., Ly, C. H. & Ryall, J. G. A metabolic link to skeletal muscle
663 wasting and regeneration. *Front Physiol* **5**, 32,
664 doi:10.3389/fphys.2014.00032 (2014).
665 54 Vatrinet, R. *et al.* The α-ketoglutarate dehydrogenase complex in cancer
666 metabolic plasticity. *Cancer Metab* **5**, 3, doi:10.1186/s40170-017-0165-0
667 (2017).
668 55 Whereat, A. F., Hull, F. E. & Orishimo, M. W. The role of succinate in the
669 regulation of fatty acid synthesis by heart mitochondria. *J Biol Chem* **242**,
670 4013-4022 (1967).
671 56 Fonnesu, A., Capaccioli, S. & Cini-Neri, G. Effects of succinate on amino
672 acid incorporation into protein during chemical carcinogenesis. *Toxicol*
673 *Pathol* **12**, 400-403, doi:10.1177/019262338401200416 (1984).

674 57 Ostergaard, E. Disorders caused by deficiency of succinate-CoA ligase. *J*
675 *Inherit Metab Dis* **31**, 226-229, doi:10.1007/s10545-008-0828-7 (2008).
676 58 Kacso, G. *et al.* Two transgenic mouse models for beta-subunit
677 components of succinate-CoA ligase yielding pleiotropic metabolic
678 alterations. *Biochem J* **473**, 3463-3485, doi:10.1042/BCJ20160594 (2016).
679 59 Leary, S. C., Battersby, B. J., Hansford, R. G. & Moyes, C. D. Interactions
680 between bioenergetics and mitochondrial biogenesis. *Biochim Biophys*
681 *Acta* **1365**, 522-530 (1998).
682 60 Moyes, C. D., Mathieu-Costello, O. A., Tsuchiya, N., Filburn, C. &
683 Hansford, R. G. Mitochondrial biogenesis during cellular differentiation.
684 *Am J Physiol* **272**, C1345-1351, doi:10.1152/ajpcell.1997.272.4.C1345
685 (1997).
686 61 Korohoda, W., Pietrzkowski, Z. & Reiss, K. Chloramphenicol, an inhibitor
687 of mitochondrial protein synthesis, inhibits myoblast fusion and myotube
688 differentiation. *Folia Histochem Cytobiol* **31**, 9-13 (1993).
689 62 Arany, Z. *et al.* The transcriptional coactivator PGC-1beta drives the
690 formation of oxidative type IIX fibers in skeletal muscle. *Cell Metab* **5**, 35-
691 46, doi:10.1016/j.cmet.2006.12.003 (2007).
692 63 Leone, T. C. *et al.* PGC-1alpha deficiency causes multi-system energy
693 metabolic derangements: muscle dysfunction, abnormal weight control
694 and hepatic steatosis. *PLoS Biol* **3**, e101,
695 doi:10.1371/journal.pbio.0030101 (2005).
696 64 Lelliott, C. J. *et al.* Ablation of PGC-1beta results in defective
697 mitochondrial activity, thermogenesis, hepatic function, and cardiac
698 performance. *PLoS Biol* **4**, e369, doi:10.1371/journal.pbio.0040369
699 (2006).
700 65 Cai, X. *et al.* Alpha-ketoglutarate promotes skeletal muscle hypertrophy
701 and protein synthesis through Akt/mTOR signaling pathways. *Sci Rep* **6**,
702 26802, doi:10.1038/srep26802 (2016).
703 66 Blomqvist, B. I., Hammarqvist, F., von der Decken, A. & Wernerman, J.
704 Glutamine and alpha-ketoglutarate prevent the decrease in muscle free
705 glutamine concentration and influence protein synthesis after total hip
706 replacement. *Metabolism* **44**, 1215-1222 (1995).
707 67 Tazi, E. & Errihani, H. Treatment of cachexia in oncology. *Indian J Palliat*
708 *Care* **16**, 129-137, doi:10.4103/0973-1075.73644 (2010).
709 68 Le-Rademacher, J. G., Crawford, J., Evans, W. J. & Jatoi, A. Overcoming
710 obstacles in the design of cancer anorexia/weight loss trials. *Crit Rev*
711 *Oncol Hematol* **117**, 30-37, doi:10.1016/j.critrevonc.2017.06.008 (2017).
712 69 Doles, J. D. *et al.* Does the Poly (ADP-Ribose) Polymerase Inhibitor
713 Veliparib Merit Further Study for Cancer-Associated Weight Loss?
714 Observations and Conclusions from 60 Prospectively Treated Patients. *J*
715 *Palliat Med*, doi:10.1089/jpm.2018.0023 (2018).
716 70 von Haehling, S., Morley, J. E., Coats, A. J. S. & Anker, S. D. Ethical
717 guidelines for publishing in the journal of cachexia, sarcopenia and
718 muscle: update 2017. *J Cachexia Sarcopenia Muscle* **8**, 1081-1083,
719 doi:10.1002/jcsm.12261 (2017).
720

721 **FIGURE LEGENDS**

722 **Figure 1: Modeling succinate accumulation and evaluating consequences**
723 **on growth and atrophy (A)** A bar graph depicting relative intracellular levels of
724 TCA metabolites in C2C12 myoblasts following 48h DM-succinate treatment as
725 determined by gas chromatography mass spectrometry (GC/MS) analyses.
726 *p<0.05. n=3 replicates. **(B)** Proliferation curve (measured as percent
727 confluence) for control, 4, 8, and 16 mM DM-succinate over 48 hours. Percent
728 confluence was averaged from 3 images per replicate, N= 6 replicate wells for
729 each condition. Error bars represent SEM. **(C)** Percent apoptotic cells, measured
730 by number of Annexin V positive cells, for control, 4, 8, and 16 mM DM-succinate
731 over 48 hours. Percent apoptotic cells was averaged from 3 images per replicate,
732 N=3 replicate wells for each condition. Error bars represent SD. **(D)** Bar graphs
733 quantifying Murf1 (left) and Atrogin1 (right) mRNA expression FC relative to D0-
734 growth media at 0, 1, 2, 3, and 4d in differentiation media +/- 8 mM DM-
735 succinate. *p<0.05 between control and succinate samples for marked
736 timepoints, as determined by multiple t tests with Holm-Sidak multiple testing
737 correction. **(E)** A bar graph showing reduced OPP accumulation in C2C12 cells
738 treated for 48h with 8mM DM-succinate. n=3 replicates; *p<0.05. **(F)** A graph of
739 myotube diameter measurements (microns) from C2C12 myotubes treated with
740 DM-succinate for 24h. n.s.=not significant (p>0.05) between any conditions
741 tested.

742 **Figure 2: Elevated succinate levels impair *in vitro* myogenesis (A)** RNA
743 sequencing analysis of proliferating C2C12 myoblasts treated with 8 mM DM-
744 succinate for 48 hours. Heatmap depicting normalized FPKM values for
745 myogenic and muscle lineage marker expression values. Blue=lower relative
746 expression, orange=higher relative expression. n=3 replicates for each condition.
747 **(B)** qPCR analysis of myogenic markers Pax7, MyoD1, Myog, and MyH1. Bar
748 graphs depicting mRNA expression FC relative to D0-growth media at 0, 1, 2, 3,
749 and 4d in differentiation media +/- 8 mM DM-succinate. n=3 replicates for each
750 timepoint/condition, *p<0.05 between control and succinate samples for marked
751 timepoints, as determined by multiple t tests with Holm-Sidak multiple testing

752 correction. **(C)** Representative images of C2C12 cultures in the presence of
753 differentiation media supplemented with 8mM DM-succinate for the entirety of
754 differentiation (5 days). Red depicts myosin heavy chain positive myocytes and
755 maturing myotubes. Nuclei are shown in blue (DAPI). Scale bar=100um. **(D)** A
756 graph depicting the number of nuclei per myosin heavy chain positive structure
757 (one point=one structure). Red=statistically significant ($p<0.05$) mean of
758 biological replicates compared to control using unpaired, nonparametric, Mann-
759 Whitney tests. n=4 replicates control/8mM DM-succinate, n=5 replicates 4mM
760 DM-succinate, 20-40 myotubes/replicate.

761 **Figure 3: Succinate supplementation impairs skeletal muscle homeostasis**
762 **(A)** Bi-weekly body weight tracking over 6-week succinate supplementation.
763 Weights are normalized to pre-supplementation baseline measures. Individual
764 points are individual animals, line represents the mean at each time point. **(B)**
765 Mouse weight at endpoint, normalized to pre-supplementation baseline
766 measures. **(C)** Bi-weekly MRI-measured lean mass normalized to pre-
767 supplementation baseline measures. Individual points are individual animals, box
768 represents the quartiles and whiskers represent the minimum and maximum
769 values. **(D)** Weights of tibialis anterior (TA) and gastrocnemius (GR) at endpoint
770 in milligrams. Individual points are individual animals, box represents the
771 quartiles and whiskers represent the minimum and maximum values. **(E)**
772 Representative images of TA muscle tissue sections from vehicle or succinate
773 supplemented mice after 6 weeks administration. Cross sections are
774 immunofluorescent stained with an antibody targeting laminin (white). Nuclei are
775 labeled with DAPI (blue). Scale bars=100 μm **(F)** Quantification of minimum feret
776 diameter of myofibers from vehicle and succinate supplemented mice. Feret
777 diameters were binned to a histogram and fit with a non-linear regression
778 (gaussian, least squares regression). Succinate exposed myofibers were
779 significantly smaller; $P< 0.0001$ by extra sun-of-squares F test. n.s. = not
780 significant by student's t test, n=7 vehicle, n=8 succinate-supplemented FVB
781 male mice, 4-5 months old at the start of the study.

782 **Figure 4: Succinate supplementation impairs skeletal muscle regeneration**

783 **(A)** Representative images of TA muscle tissue sections from vehicle or
784 succinate supplemented mice 7 days post 1.2% $BaCl_2$ injury stained with an
785 antibody targeting laminin (white). Nuclei are labeled with DAPI (blue). **(B)** A
786 histogram of myofiber feret diameters at 7 days post injury (dpi). Non-linear
787 regression and statistical analyses were performed as in Fig. 3, succinate injured
788 myofibers were ~16% smaller; p=0.0016. **(C)** Representative images of TA
789 muscle tissue sections from vehicle or succinate supplemented mice 28 days
790 post 1.2% $BaCl_2$ injury stained with an antibody targeting laminin (white). Nuclei
791 are labeled with DAPI (blue). **(D)** A histogram of myofiber feret diameters at 28
792 days post injury (dpi). Non-linear regression and statistical analyses were
793 performed as in Fig. 3, succinate injured myofibers were ~52% smaller;
794 p<0.0001. **(E)** Representative images of TA muscle tissue sections from vehicle
795 or succinate supplemented mice 28 dpi stained with antibodies targeting Pax7
796 (green), and Ki67 (red, upper panels), or Myogenin (red, lower panels). Nuclei
797 are labeled with DAPI (blue). Yellow arrows in upper panels point to Pax7+/Ki67+
798 cells. Yellow arrow heads in lower panels point to Myog+ cells. **(F)** Quantification
799 of Pax7+, Pax7+/Ki67+, and Myog+ cells per mm^2. Data represent the
800 quantification of a 0.844 mm^2 area per animal. Data points represent individual
801 animals. Box represents the inner quartiles and whiskers represent minimum and
802 maximum values. p values are represented in the figure, as determined by
803 unpaired student's t test. Mice were 3-4 months old, FVB males. n=5 mice 28dpi
804 vehicle; n=4 mice 28dpi succinate; n=5 mice 7dpi vehicle; n=3 mice 7dpi
805 succinate. Scale bars in panel 4A and 4C=100 um, 4E=50 µm.

806 **Figure 5: Succinate elevation impairs mitochondria function in myoblast**
807 **cells (A)** A bar chart depicting pathway enrichment analyses (sorted by p-value)
808 using HMDB IDs. Shown are the top 25 enriched processes. All data are derived
809 from Metaboanalyst processing of non-targeted analysis of C2C12 cells treated
810 with control or 8 mM DM-succinate media for 48 hours. n=3 control and n=3 8
811 mM DM-succinate. **(B)** A circular pie chart depicting the relative distribution of
812 differentially regulated metabolic pathways using HMDB IDs during function
813 explorer analysis. **(C)** Line graphs showing oxygen consumption rates (OCR),

814 normalized to cell count, of C2C12 myoblasts treated sequentially with
815 oligomycin (dashed line 1), FCCP (dashed line 2), and Antimycin A/Rotenone
816 (dashed line 3) in the presence or absence of 4 mM or 8 mM DM-succinate. **(D-**
817 **G)** Bar graphs displaying basal respiration rates (F), maximal respiration (G),
818 reserve capacity (H), and non-mitochondrial respiration (I). n=3; *$p<0.05$,
819 **$p<0.01$ by unpaired student's t-test**. (H)** Line graphs depicting OCR and ECAR
820 (extracellular acidification rate) in response to mitochondria stress (Energy
821 phenotype assay; Seahorse) in C2C12 control or DM-succinate treated
822 myoblasts. Filled circles are basal conditions, open circles are stressed
823 conditions. n=3 control and n=3 8 mM succinate.

Figure 1

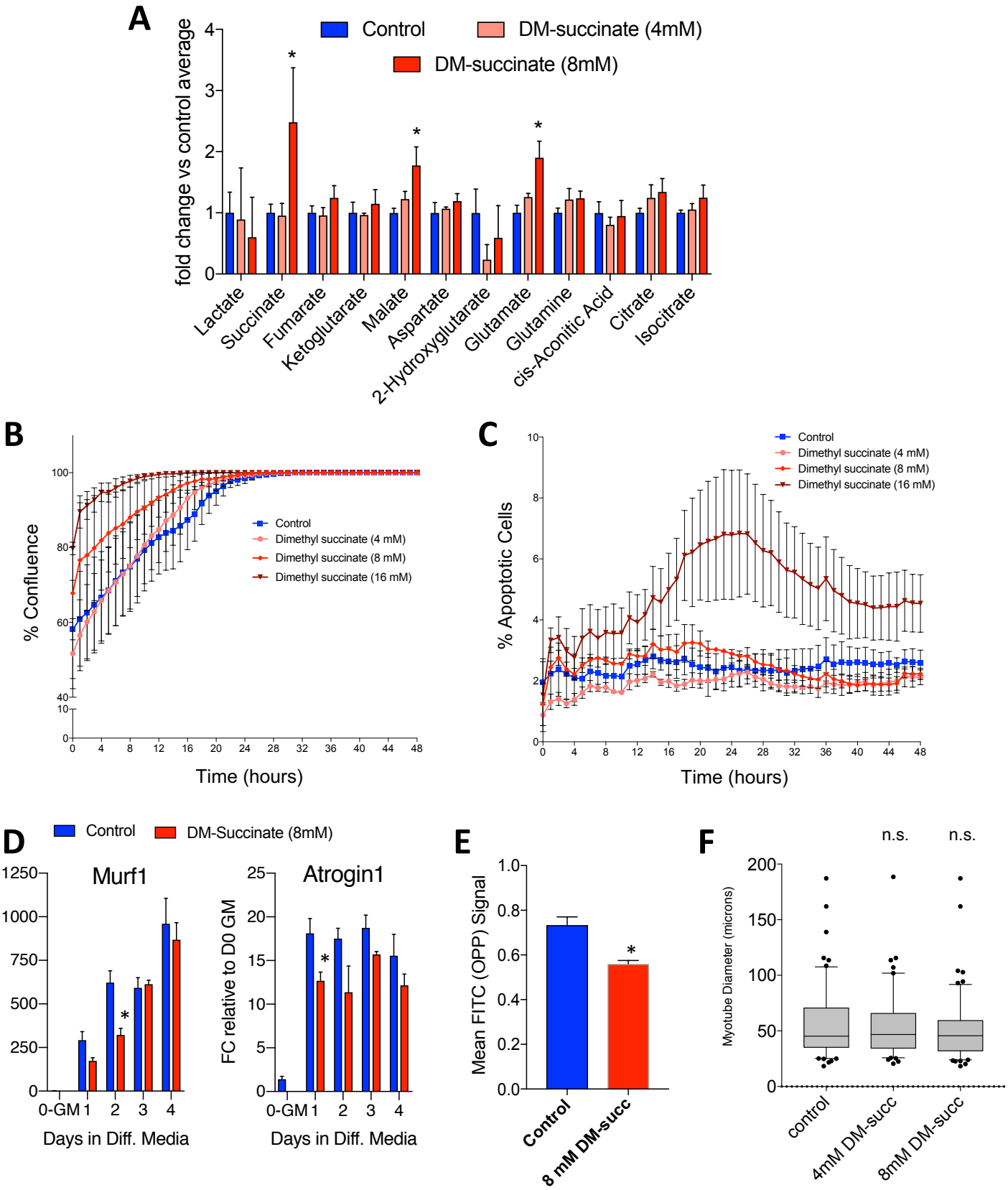
A
Control
DM-succinate (4mM)
DM-succinate (8mM)
fold change vs control average
Lactate
Succinate
Fumarate
Ketoglutarate
Malate
Aspartate
2-Hydroxyglutarate
Glutamate
Glutamine
cis-Aconitic Acid
Citrate
Isocitrate
B
% Confluence
Time (hours)
Control
Dimethyl succinate (4 mM)
Dimethyl succinate (8 mM)
Dimethyl succinate (16 mM)
C
% Apoptotic Cells
Time (hours)
Control
Dimethyl succinate (4 mM)
Dimethyl succinate (8 mM)
Dimethyl succinate (16 mM)
D
Control
DM-Succinate (8mM)
Murf1
Atrogin1
FC relative to D0 GM
Days in Diff. Media
E
Mean FITC (OPP) Signal
Control
8 mM DM-succ
F
n.s.
n.s.
Myotube Diameter (microns)
control
4mM DM-succ
8mM DM-succ

Figure 2

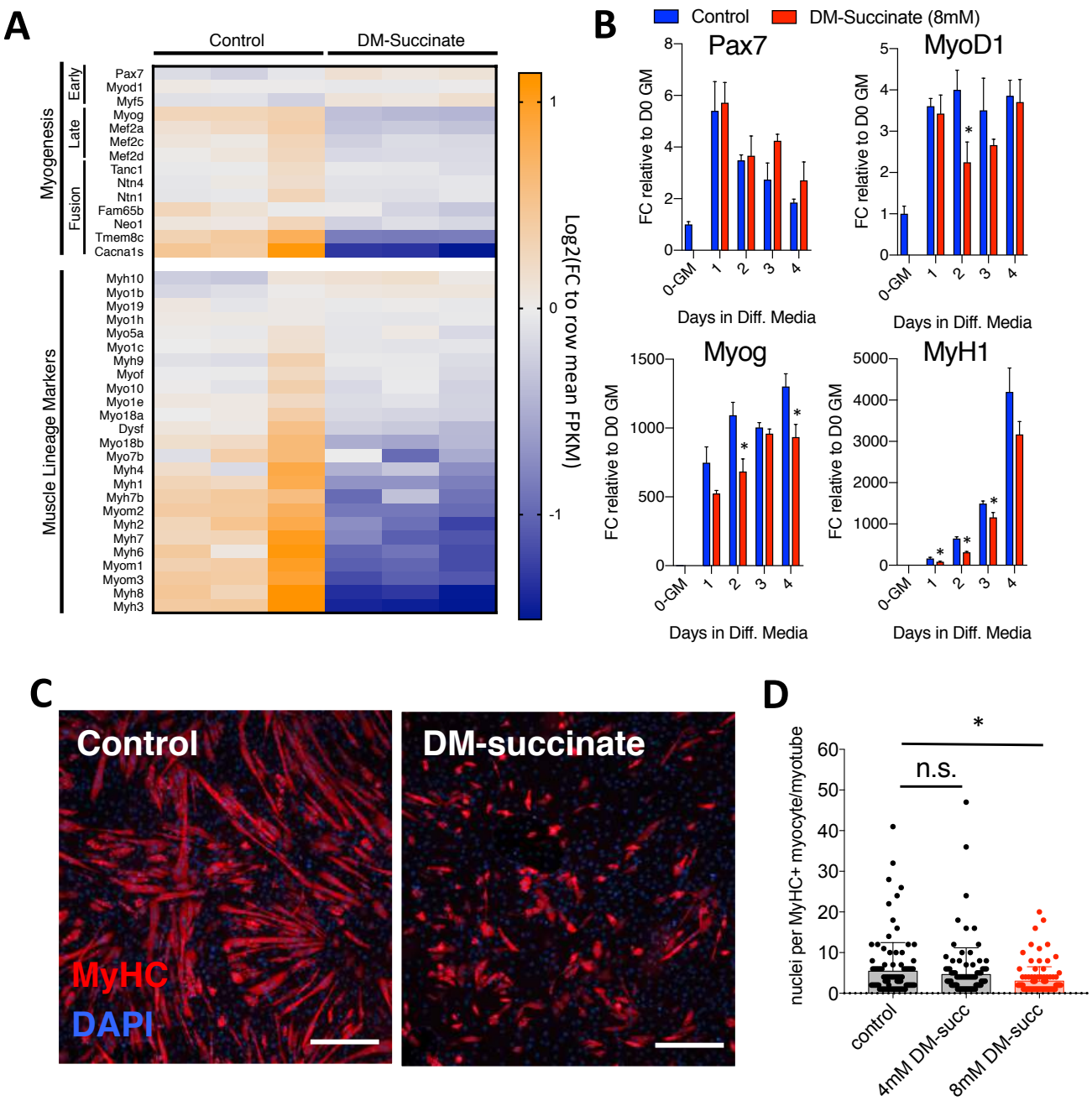
A
Control
DM-Succinate
Myogenesis
Early
Late
Fusion
Muscle Lineage Markers
Pax7
Myod1
Myf5
Myog
Mef2a
Mef2c
Mef2d
Tanc1
Ntn4
Ntn1
Fam65b
Neo1
Tmem8c
Cacna1s
Myh10
Myo1b
Myo19
Myo1h
Myo5a
Myo1c
Myh9
Myof
Myo10
Myo1e
Myo18a
Dysf
Myo18b
Myo7b
Myh4
Myh1
Myh7b
Myom2
Myh2
Myh7
Myh6
Myom1
Myom3
Myh8
Myh3
Log2(FC to row mean FPKM)
1
0
-1
B
Control
DM-Succinate (8mM)
Pax7
MyoD1
Myog
MyH1
FC relative to D0 GM
Days in Diff. Media
0-GM
1
2
3
4
C
Control
DM-succinate
MyHC
DAPI
D
nuclei per MyHC+ myocyte/myotube
n.s.
*
control
4mM DM-succ
8mM DM-succ

Figure 3

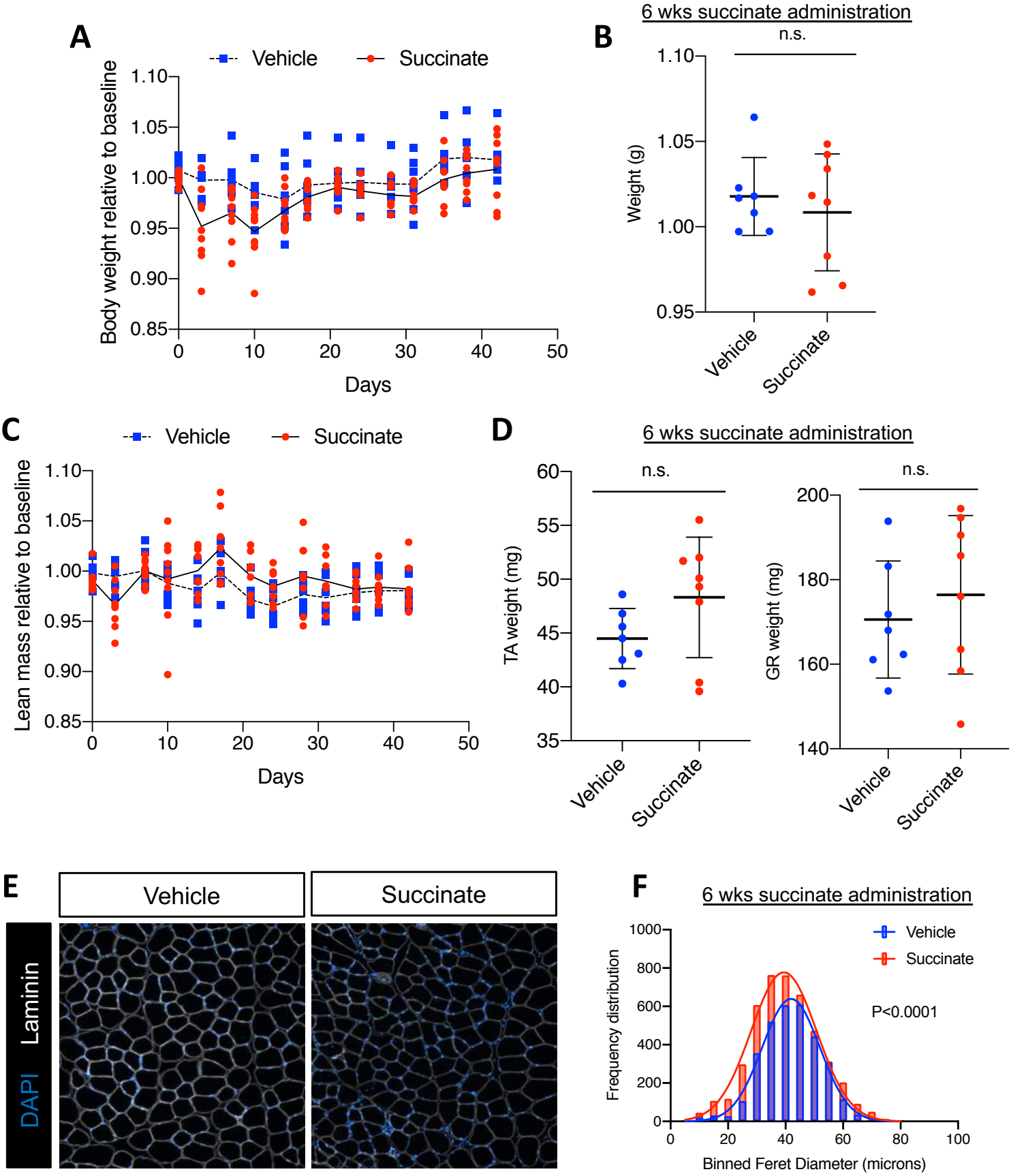
A
Vehicle
Succinate
Body weight relative to baseline
1.10
1.05
1.00
0.95
0.90
0.85
0
10
20
30
40
50
Days
B
6 wks succinate administration
n.s.
Weight (g)
1.10
1.05
1.00
0.95
Vehicle
Succinate
C
Vehicle
Succinate
Lean mass relative to baseline
1.10
1.05
1.00
0.95
0.90
0.85
0
10
20
30
40
50
Days
D
6 wks succinate administration
n.s.
TA weight (mg)
60
55
50
45
40
35
Vehicle
Succinate
n.s.
GR weight (mg)
200
180
160
140
Vehicle
Succinate
E
Vehicle
Succinate
Laminin
DAPI
F
6 wks succinate administration
Vehicle
Succinate
P<0.0001
Frequency distribution
1000
800
600
400
200
0
0
20
40
60
80
100
Binned Feret Diameter (microns)

Figure 4

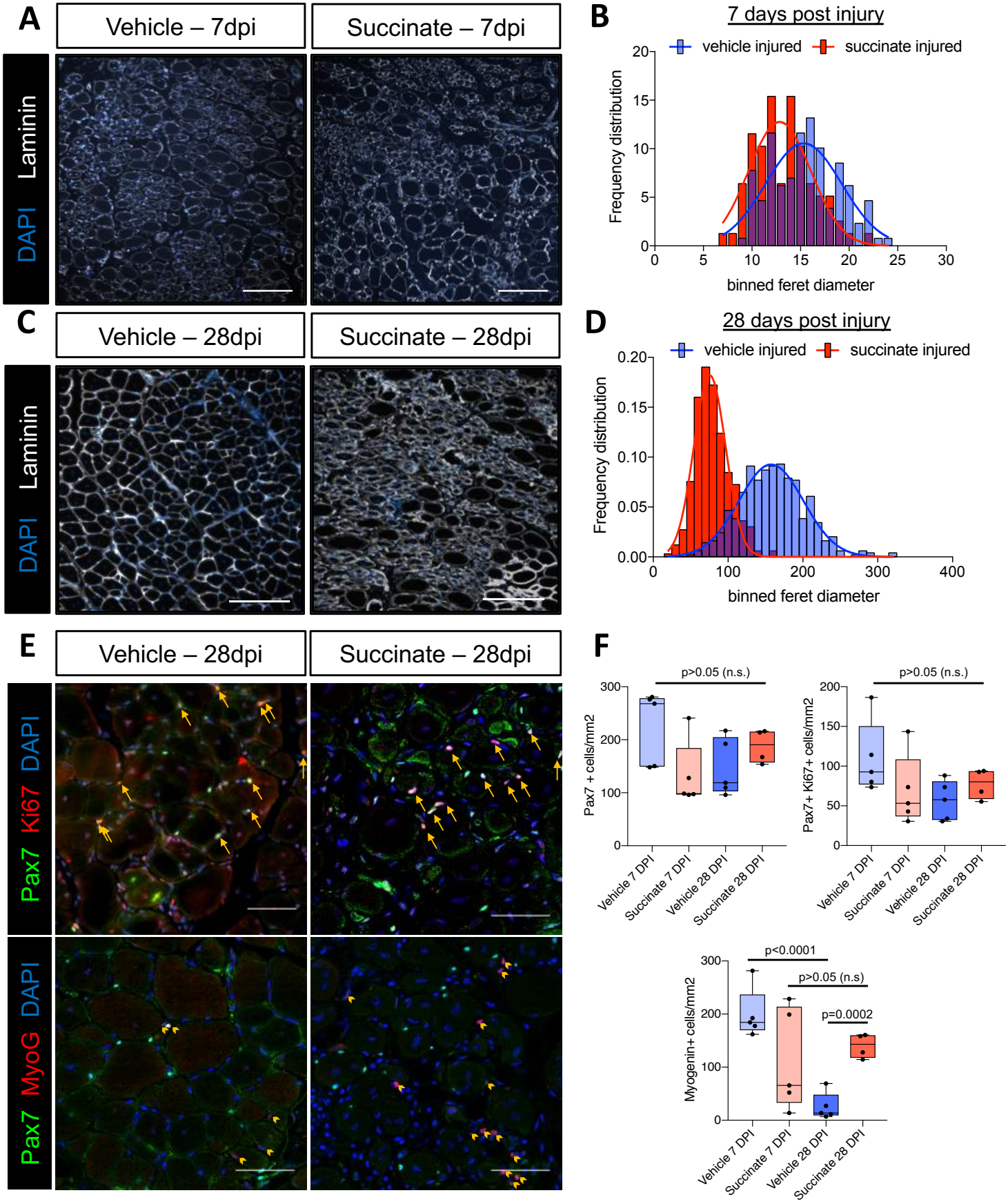
A
Vehicle – 7dpi
Succinate – 7dpi
Laminin
DAPI
B
7 days post injury
vehicle injured
succinate injured
Frequency distribution
binned feret diameter
C
Vehicle – 28dpi
Succinate – 28dpi
Laminin
DAPI
D
28 days post injury
vehicle injured
succinate injured
Frequency distribution
binned feret diameter
E
Vehicle – 28dpi
Succinate – 28dpi
Pax7 Ki67 DAPI
Pax7 MyoG DAPI
F
p>0.05 (n.s.)
Pax7 + cells/mm2
p>0.05 (n.s.)
Pax7+ Ki67+ cells/mm2
p<0.0001
p>0.05 (n.s)
p=0.0002
Myogenin+ cells/mm2
Vehicle 7 DPI
Succinate 7 DPI
Vehicle 28 DPI
Succinate 28 DPI

Figure 5

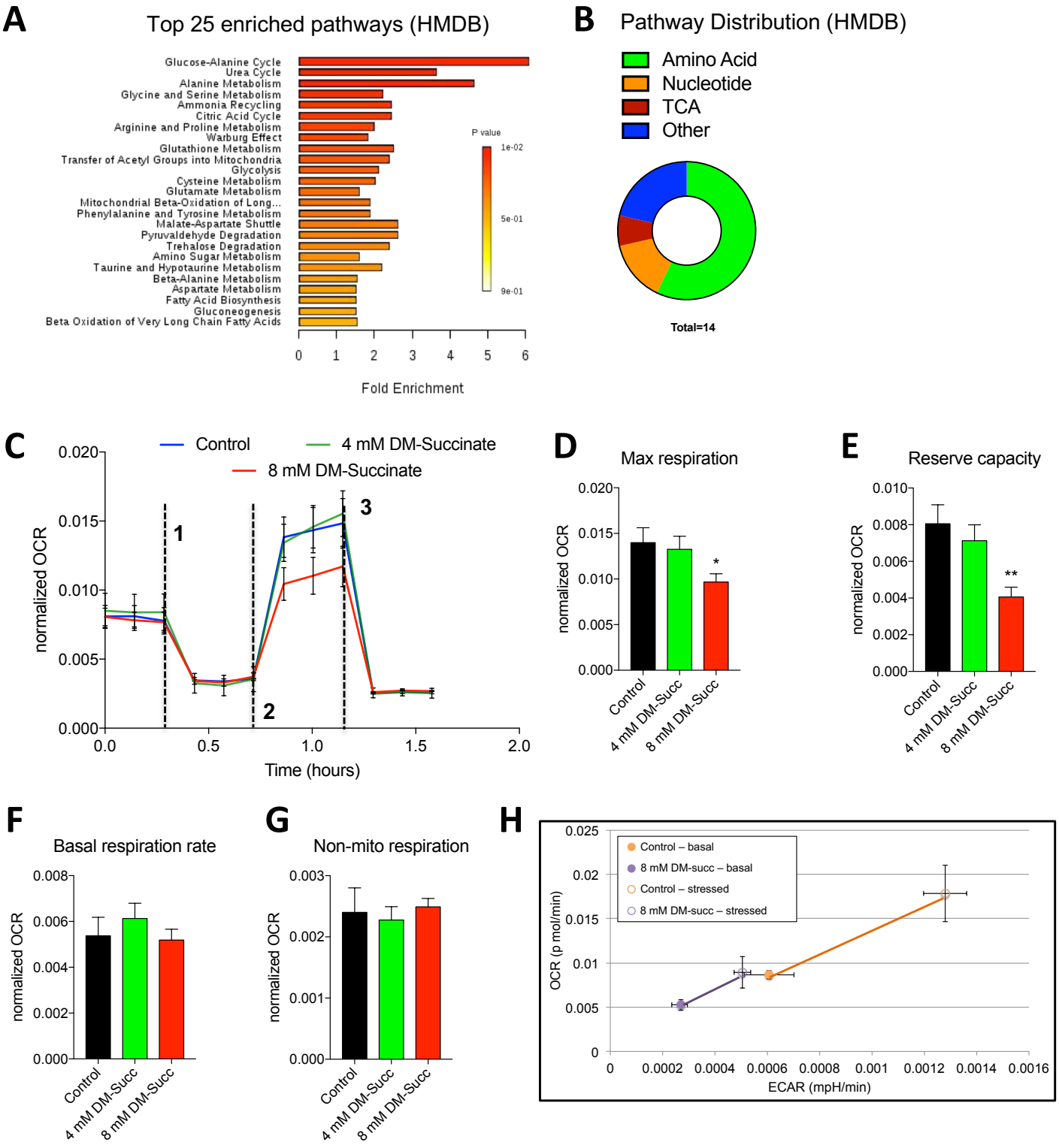
A
Top 25 enriched pathways (HMDB)
Glucose-Alanine Cycle
Urea Cycle
Alanine Metabolism
Glycine and Serine Metabolism
Ammonia Recycling
Citric Acid Cycle
Arginine and Proline Metabolism
Warburg Effect
Glutathione Metabolism
Transfer of Acetyl Groups into Mitochondria
Glycolysis
Cysteine Metabolism
Glutamate Metabolism
Mitochondrial Beta-Oxidation of Long...
Phenylalanine and Tyrosine Metabolism
Malate-Aspartate Shuttle
Pyruvaldehyde Degradation
Trehalose Degradation
Amino Sugar Metabolism
Taurine and Hypotaurine Metabolism
Beta-Alanine Metabolism
Aspartate Metabolism
Fatty Acid Biosynthesis
Gluconeogenesis
Beta Oxidation of Very Long Chain Fatty Acids
P value
1e-02
5e-01
9e-01
0 1 2 3 4 5 6
Fold Enrichment
B
Pathway Distribution (HMDB)
Amino Acid
Nucleotide
TCA
Other
Total=14
C
Control
4 mM DM-Succinate
8 mM DM-Succinate
normalized OCR
0.020
0.015
0.010
0.005
0.000
1
2
3
0.0 0.5 1.0 1.5 2.0
Time (hours)
D
Max respiration
normalized OCR
0.020
0.015
0.010
0.005
0.000
*
Control
4 mM DM-Succ
8 mM DM-Succ
E
Reserve capacity
normalized OCR
0.010
0.008
0.006
0.004
0.002
0.000
**
Control
4 mM DM-Succ
8 mM DM-Succ
F
Basal respiration rate
normalized OCR
0.008
0.006
0.004
0.002
0.000
Control
4 mM DM-Succ
8 mM DM-Succ
G
Non-mito respiration
normalized OCR
0.003
0.002
0.001
0.000
Control
4 mM DM-Succ
8 mM DM-Succ
H
Control – basal
8 mM DM-succ – basal
Control – stressed
8 mM DM-succ – stressed
OCR (p mol/min)
0.025
0.02
0.015
0.01
0.005
0
0 0.0002 0.0004 0.0006 0.0008 0.001 0.0012 0.0014 0.0016
ECAR (mpH/min)